Acta Cryst. (1994). D**50**, 210-218

Analysis of Diffuse Scattering from Yeast Initiator tRNA Crystals

BY ANAND R. KOLATKAR, JAMES B. CLARAGE AND GEORGE N. PHILLIPS JR

Department of Biochemistry and Cell Biology and W. M. Keck Center for Computational Biology, Rice University, PO Box 1892, *Houston, TX* 77251-1892, *USA*

(*Received* 6 *March* 1993; *accepted* 21 *October* 1993)

Abstract

Yeast initiator tRNA crystals exhibit strong X-ray diffuse scattering. This scattering can be used to extract information about lattice-coupled and intramolecular motions in the crystals. The amplitudes and correlation distances of these motions can be estimated by calculating the diffuse scattering and comparing the results with the observed scattering. Results indicate that both anisotropic, lattice-coupled motions as well as short-range correlated local disorder in the anticodon arm contribute to the overall disorder in the crystals. These types of motions can be correlated with aspects of tRNA function. This additional information complements the results from analysis of crystallographic data and provides a more detailed picture of the structure and dynamics of the molecule. The degree to which the methodology presented here can account for the observed diffuse scattering from tRNA represents a significant step forward in the ability to use this conventionally discarded information, and encourages the ultimate extension of these ideas to a wide variety of macromolecular systems.

Introduction

X-ray crystal structure analysis can provide great detail about the average structure of a macromolecule. During the refinement process, regions of the molecule are sometimes found to be disordered; high B values and poorly defined electron density indicate the absences of single well ordered conformations. To analyze the structure further, crystallographers have modeled alternate conformations and ensembles of structures to fit the Bragg data better (Kuriyan *et al.*, 1991; Gros, van Gunsteren & Hol, 1990; Clarage & Phillips, 1994). The Bragg data used in each of these refinement techniques, however, contain no information about the correlations in the disorder. Information in the form of diffuse, or variational, X-ray scattering is excluded from the usual structural analysis scheme for proteins and nucleic acids. This unused scattering contains the information about inter- and intramolecular motions and their correlations in the crystal.

X-ray diffuse scattering cannot generally be used to differentiate between static and dynamic disorder. Dynamic disorder can often be distinguished by changing the temperature of the system. Decreasing the temperature during data collection often results in an increase in the resolution and intensity of the high-angle Bragg reflections, indicating increased ordering in the crystals (Phillips, Fillers & Cohen, 1980; Frauenfelder, Petsko & Tsernoglou, 1979; Parak *et al.*, 1987). Experimental evidence supporting significant dynamic disorder within macromolecular crystals has been reviewed by Petsko & Ringe (1984). Moreover, inelastic diffuse scattering experiments on myoglobin crystals using a Mössbauer radiation source demonstrated that much of the disorder in crystals is indeed dynamic (Nienhaus, Heinzland, Huenges & Parak, 1989). Such data are not available for the yeast initiator tRNA crystals. However, based on the data from protein crystals, it seems clear that much of the disorder seen in tRNA crystals must be dynamic. Even if the interconversion of conformations within crystallized tRNA molecules does not occur on fast time scales, diffuse scattering studies still reveal the conformational flexibility of the molecules, which is crucial to understanding their biological function.

Application of diffuse scattering analysis to protein and nucleic acid crystals has provided information about a variety of systems. Although diffuse scattering intensities cannot be Fourier-inverted to produce directly the description of the motions, diffuse scattering can be calculated from models and compared with experimental results to yield insights about the macromolecular motions. Analysis of tropomyosin crystals reveals considerable motion in the filamentous protein lattice (Boylan & Phillips, 1986; Chacko & Phillips, 1992). Similarly, globular protein crystals have also been analyzed for diffuse scattering. Insulin crystals have been shown to contain movements that are predominantly correlated over distances of approximately 6 Å (Caspar, Clarage, Salunke & Clarage, 1988). Short-range correlated motions have also been found to dominate in triclinic and tetragonal lysozyme crystals (Clarage, Clarage, Phillips, Sweet & Caspar, 1992). Orthorhombic lysozyme crystals produce diffuse streaks which have been calculated by a long-range lattice-coupled model (Doucet & Benoit, 1987). Diffuse scattering from crystals of a DNA octamer revealed partially disordered B-DNA present in the solvent channels formed by A-DNA (Doucet, Benoit, Cruse, Prange & Kennard, 1989).

The studies on lysozyme and insulin share some assumptions. First, a certain homogeneity in the disorder is assumed in the diffuse scattering studies mentioned above. That is, all parts of the molecule are assumed to undergo the same specified disorder. The limitation in this assumption is that diffuse scattering from a portion of the molecule cannot be modeled by these methods. Furthermore, correlations have been modeled as isotropically distributed disorder. These assumptions are valid in some cases but may not always apply.

In this study, we describe the analysis of X-ray diffuse scattering from yeast initiator transfer RNA (tRNA) crystals. The analysis shows that the assumptions of homogeneous and isotropic disorder do not suffice in this case. Therefore, existing techniques have been modified and extended to overcome these assumptions.

The structure of yeast initiator tRNA (space group $P6_422$) has been solved to 3 Å resolution (Basavappa, 1991; Basavappa & Sigler, 1991) (see Fig. 1). The 3′-end of this nucleic acid molecule forms a complex with the amino acid, methionine, and is called the acceptor stem. The end of the other arm of this L-shaped molecule is responsible for the specificity in the binding of the tRNA to messenger RNA (mRNA) in the ribosome; the three bases (or anticodon) on the tip of this arm interact with the codon bases on mRNA. In the crystal, the acceptor arms of adjacent tRNA molecules line up to form a pseudo-helix along the *c* axis of the unit cell with the anticodon arms extending out almost perpendicularly from this pseudo-helix axis (see Figs. 2*c* and 3*c*). Adjacent pseudo-helices contact each other through their extended anticodon loops. The electron density for the anticodon loop region, however, is not localized, and *B* values can be greater than 100 Å^2

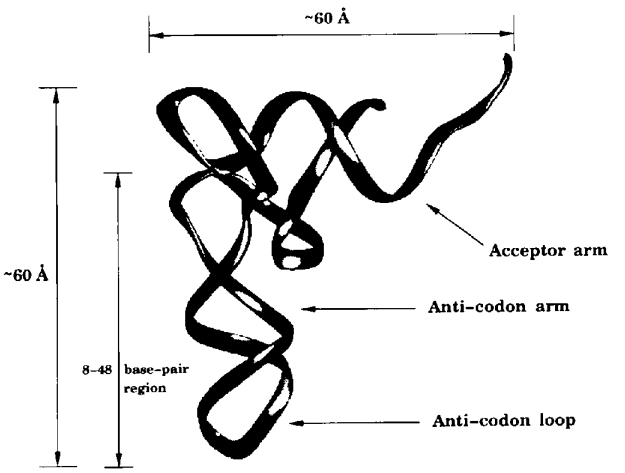

Fig. 1. Ribbon drawing of one yeast initiator tRNA molecule using *RIBBONS* (Carson, 1987). Note the double-helical character in the acceptor stem and anticodon regions. Aminoacylated amino acids are attached to the 3′-OH end of the acceptor stem. The three nucleic acid bases that provide the base-pairing specificity for the start codon on the messenger RNA are located at the tip of the anticodon loop.

corresponding to r.m.s. displacements of the order of 1 Å. The solvent content in this crystal form is high (approximately 82%) indicating that there is room for large-scale molecular motions in the unit cell.

Diffuse scattering features

The basic diffuse scattering features from yeast initiator tRNA have been described previously (Kolatkar, Phillips, Basavappa & Sigler, 1990; Glover, Harris, Helliwell & Moss, 1991). Preliminary analysis of this diffuse intensity has been carried out to obtain specific details about the disorder (Kolatkar, Clarage & Phillips, 1992). The data used in the current analysis have been collected on imaging plates using synchrotron radiation at the Photon Factory (Japan) (Basavappa & Sigler, 1991). The diffraction from these crystals reveals various forms of diffuse scattering. The most striking of these features are the streaks seen in the diffraction images in Figs. 2(*a*) and 3(*a*).

The orientation of the streaks of diffuse scattering can be correlated with the packing of molecules in the crystal. Fig. 2(*a*) shows an image of tRNA X-ray scattering which corresponds to the unit-cell orientation shown in Fig. 2(*c*). In the diffraction image, the c^* axis runs from the lower left corner to the upper right corner. In the unit-cell drawing, the *c* axis runs in the same direction. Similarly, Fig. 3(*a*) shows the diffraction data corresponding to the unit-cell orientation in Fig. 3(*c*). In both views, the diffuse streaks run perpendicular to the c^* axis and also to the pseudo-helix lying along the *c* axis. If some part of the molecule were moving parallel to the *c* axis, diffuse scattering situated along the c^* axis would be expected. It is possible to estimate the correlation distances for this component of the diffuse scattering by judging the dimensions of the streaks in reciprocal ångströms and inverting. To refine these correlation distances, the diffuse scattering from such a model is calculated and compared to the actual diffraction data. The correctness of the model is determined by the degree of similarity between the calculated and observed diffuse scattering.

Other features seen in the diffraction images are the very diffuse clouds of scattering. The location of the clouds, the bulk of which lie in the *hk*0 plane in the 3-3.5 Å resolution range, together with the fact that the disordered anticodon loops lie perpendicular to the *c* axis, suggest that this component is the result of motion in the anticodon region. Because this diffuse feature is not associated with Bragg positions and is smoothly varying, the disorder producing this scattering is some type of short-range correlated motion. The fact that these clouds are not continuous around the reciprocal origin suggests that the global 6 Å coupling model used for the intramolecular displacements in globular proteins may not be valid for tRNA.

Computational procedures

The rationale behind these calculations is to reproduce the diffuse scattering features. Once the calculation is made to match the observed diffraction, the parameters used in the calculation provide specific information about the nature of the disorder producing the diffuse features. The quality of fit between the calculated and observed diffuse scattering from macromolecular crystals is currently judged visually as opposed to quantitatively.

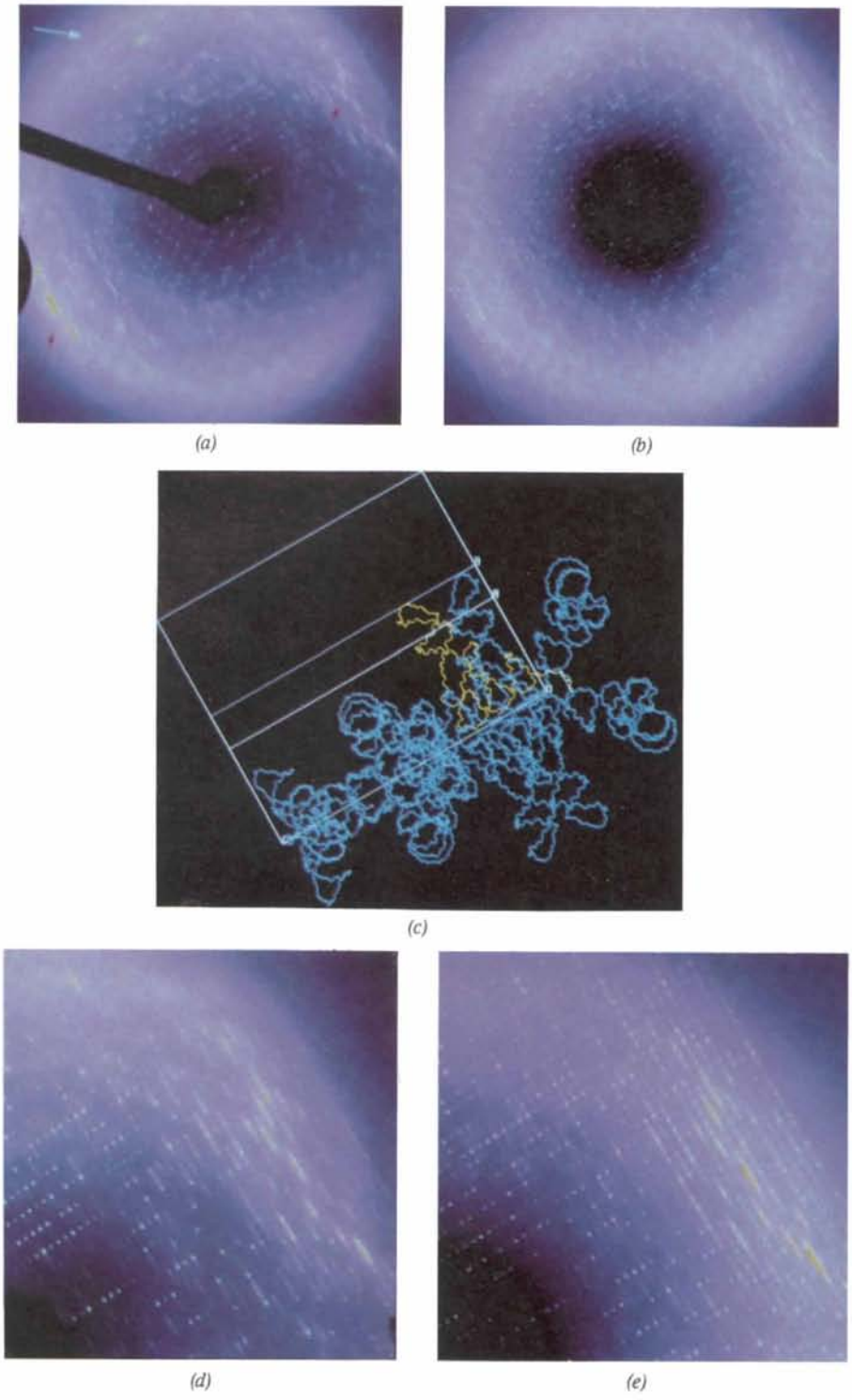

Fig. 2. Calculations of the X-ray scattering from yeast initiator tRNA crystals. The experimental image, (*a*), corresponds to a 1.5° rotation photograph recorded on an imaging plate set 200 mm from the crystal using 1.3 Å radiation. The red arrows point to the streaks elongated perpendicular to the *c* axis, which, in the calculated image, (*b*), are modeled as lattice-coupled motions along the pseudo-helix axis. The white arrow points to the very diffuse cloud which is modeled as local intramolecular motion in the anticodon arm. The corresponding unit-cell orientation is shown in (*c*) with a single tRNA molecule colored yellow and the symmetry-related molecules and unit-cell outline in blue. Magnifications of the top right quadrant from the experimental and calculated diffraction images are shown in (*d*) and (*e*), respectively. The upper right-hand quadrant of each of these images shows a close correspondence in the diffuse intensity. The magnified images have been globally rescaled slightly to correct for the absorption seen in the lower right quadrant in image (*a*). The experimental diffraction and the diffuse scattering calculations are colored such that the least intense features appear blue, intermediate intensities pink, and the most intense features yellow. The lack of circularly symmetric intensity in the experimental image, (*a*), is partially accounted for by significant absorption.

This is not due to a lack of information in the data but rather that reliable quantitative methods are not yet available. Two different complementary methods were used to calculate the diffuse scattering from various models for the atomic disorder: the convolution method and the multi-cell method.

Convolution method

Assume that the atomic displacements are homogeneous and can be factored into statistically independent components, δ_i (*e.g.* intermolecular, intramolecular, *etc.*), where δ_i is a vector with direction and magnitude characterizing the ith component of motion. Then to lowest order, the diffuse scattering from each component can be expressed as a convolution of the ideal structure factors with the Fourier transform of an atomic displacement correlation function. Explicitly (Clarage, Clarage, Phillips, Sweet & Caspar, 1992),

$$I(\mathbf{R}) = \exp\Big[-\sum_i (2\pi\mathbf{R}\cdot\delta_i)^2\Big] \sum_i (2\pi\mathbf{R}\cdot\delta_i)^2 \times \big\{F_o^2(\mathbf{R}) * \mathrm{FT}\big[\Gamma_i(\mathbf{r})\big]\big\}, \quad (1)$$

where $\mathbf{R}$ is the reciprocal space vector with magnitude $(2\sin\theta/\lambda)$. $F_o^2(\mathbf{R})$ is the intensity calculated as the square of the ideal structure factor using the atomic coordinates (at their average position) with no B values. The correlation function, $\Gamma_i(\mathbf{r})$,† describes how displacements along the component δ_i are correlated for atomic separations, $\mathbf{r}$.

The total diffuse scattering is actually given by a power series in $(2\pi\mathbf{R}\cdot\delta_i)^2$. At resolutions of interest in this study (3–4 Å), however, second- and higher-

† $\Gamma_i(\mathbf{r}) = \langle\delta_i(\mathbf{r}')\delta_i(\mathbf{r}' + \mathbf{r})\rangle_{\mathbf{r}'}$ where $\langle\rangle_{\mathbf{r}'}$ is a normalized average over all atomic locations $\mathbf{r}'$.

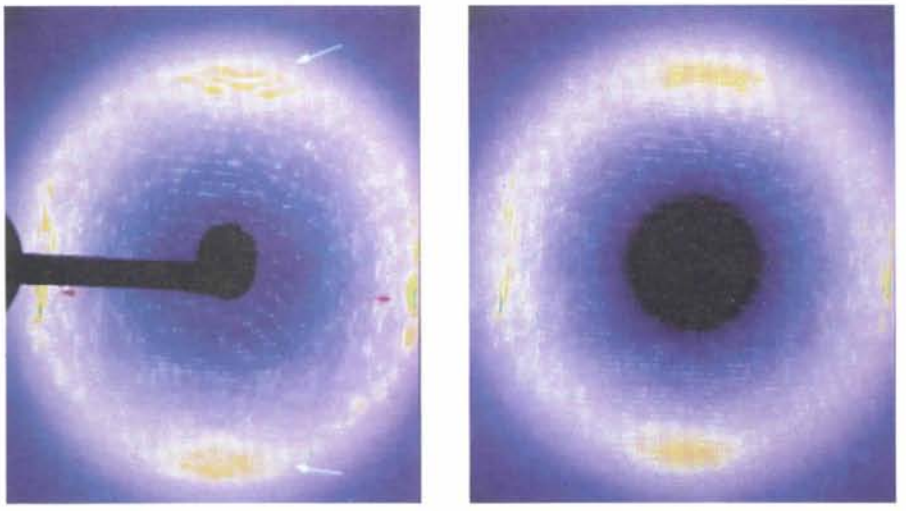

(*a*) (*b*)

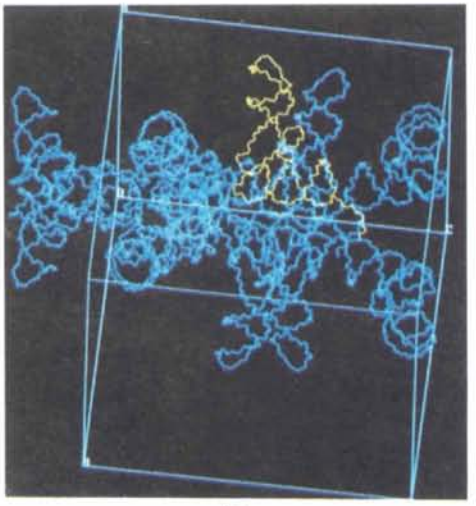

(*c*)

Fig. 3. Calculation of diffuse scattering from another tRNA crystal orientation. The experimental image is shown in (*a*), the calculated image in (*b*), and the unit-cell orientation in (*c*). The experimental parameters are the same as in Fig. 2 except that 1.17 Å radiation was used. The parameters used in the diffuse scattering calculations were identical to those in Fig. 2. Again, the red arrows point to the streaks elongated perpendicular to the c axis, which, in the calculated image, (*b*), are modeled as lattice-coupled motions along the pseudo-helix axis, while the white arrows point to the very diffuse clouds which are modeled as local intramolecular motion in the anticodon arm.

order terms should contribute only a small fraction compared to the first-order term above (Clarage, Clarage, Phillips, Sweet & Caspar, 1992). Explicit second-order calculations carried out for the tRNA data verified that the first-order approximation suffices for tRNA.

The form of the displacement correlation function, and thus that of the halo function, $\mathsf{FT}[\Gamma(\mathbf{r})]$, surrounding Bragg peaks, determines the diffuse scattering distribution in reciprocal space. If the characteristic width of Γ is less than a lattice constant, corresponding to intramolecular movements, the halos will overlap to yield a smoothly varying ring with modulations proportional to the range over which the movements are correlated. Conversely, if the characteristic width of Γ exceeds a lattice constant, the diffuse scattering consists of halos or streaks clearly associated with the Bragg reflections. A spherically symmetric exponentially decaying function, $\Gamma(\mathbf{r}) = \exp(-r/\gamma)$, produces spherical halos. It is clear from the diffraction data that the streaks are not spherically symmetrical about the Bragg positions. A possible re-parameterization of the exponential for anisotropic correlations is

$$\Gamma(\mathbf{r}) = \exp\left[-\left(\frac{r_x^2}{\gamma_x^2} + \frac{r_y^2}{\gamma_y^2} + \frac{r_z^2}{\gamma_z^2}\right)^{1/2}\right]. \qquad (2)$$

The values of γ_x, γ_y and γ_z, which are the coupling distances along three orthogonal axes, can now be adjusted separately to match the observed halo shape.

An advantage of this convolution (or Patterson) based formalism is that being analytic, there are only a handful of adjustable parameters, particularly the correlation distances and mean-squared displacements. The primary disadvantage is that only homogeneous disorder can be modeled. That is, for each component of the disorder, the entire molecule is subject to the same global Γ for all atoms. In this study, we extend this model to include non-homogeneous disorder of a specific part of the molecule which moves independently of the rest of the structure. To this end, the convolution method described above is still used but now only the atoms from a specified portion of the molecule are used in the ideal structure-factor calculation.

Multi-cell method

An alternative method for calculating the diffuse scattering was used for models which are not homogeneous. The total scattered intensity is given exactly by

$$I_T(R) = \langle|\mathsf{FT}\rho(r)|^2\rangle. \qquad (3)$$

The most general equation for the diffuse scattering intensity is therefore,

$$I_D(R) = \langle|\mathsf{FT}\rho(r)|^2\rangle - |\mathsf{FT}\langle\rho(r)\rangle|^2, \qquad (4)$$

which is simply the difference between the total and Bragg scattering; the symbol $\langle\rangle$ denotes an ensemble average in which the atoms in each molecule are displaced from their average position according to some model of motion (obtained from normal mode analysis, molecular dynamics, domain movements, *etc.*). If very long-range motions are to be examined, the electron density consists of a contiguous three-dimensional block (termed a supercell) of unit cells allowing for correlation distances greater than the unit-cell dimensions. This method was introduced to analyze the diffuse scattering from tropomyosin crystals (Boylan & Phillips, 1986; Chacko & Phillips, 1992). If the correlations are local to the unit cell, then electron density from a single unit cell is used to calculate the diffuse scattering using equation (4). This single-cell version of the method was used to calculate the diffuse scattering from the low frequency hinge-bending mode in lysozyme (Clarage, Clarage, Phillips, Sweet & Caspar, 1992). Here the total scattering, $\langle|\mathsf{FT}\rho(r)|^2\rangle$, is calculated by Fourier-transforming each unit cell, squaring the result, and then averaging over all unit cells. Similarly, the Bragg scattering, $|\mathsf{FT}\langle\rho(r)\rangle|^2$, is calculated by first averaging the electron density over all unit cells and then Fourier-transforming and squaring this average.

A final step in both the convolution and multi-cell methods involves the projection of all calculated intensities intersecting the Ewald sphere (oriented to match the diffraction image orientation) onto the film plane. These projections are compared to the diffraction images to determine the quality of the calculation. Aspects of these methods are being incorporated into a general purpose software package for diffuse scattering analysis called *XCADS* (X-ray crystallographic analysis of diffuse scattering).

Results and discussion

The diffuse scattering provides information regarding the directions of motions as well as the lengths and directions of correlations in atomic displacements. Calculations of two separate diffraction images are presented. One image was chosen such that the diffuse features were readily apparent. A second orientation was then calculated to test the global applicability of our model to any given tRNA crystal orientation. The total scattering for these two views includes six components: Bragg intensity; bulk water diffraction; independent atom motion; long-range lattice-coupled motion along the *c* axis; long-range lattice-coupled motion perpendicular to the *c* axis; short-range motion local to the anticodon arm. All these components (except the Bragg intensity) are displayed separately in Fig. 4. Each of the components was scaled individually and then summed to give the calculated images in Figs. 2(*b*) and 3(*b*). The same individual scale factors were used in the calculation of both views, a result which attests to the validity of the model in three-dimensional reciprocal space. The physical interpretation of the relative scale factors, which

are related to the relative magnitudes of the component mean-square displacements, is discussed below.

Experimental X-ray intensity curves for bulk water were used to produce the water diffraction component seen in Fig. 4 (Morgan & Warren, 1938). The tRNA crystals contain approximately 82% water, contributing significantly to the spherically symmetric scattering. Inclusion of this component provides a better fit to the observed diffraction at higher resolutions (3–4 Å).

The diffraction from an all-atom independent motion model using the multi-cell method produces spherically symmetric diffraction. Specifically, the electron density, $\rho(r)$, is built assuming a three Gaussian approximation of the atomic scattering factor for each atom (Ten Eyck, 1977; Forsyth & Wells, 1959). This component contains the calculated diffraction from a model in which each atom in tRNA moves randomly and also independently of every other atom. While this scattering may appear, on first glance, to be similar to diffraction by water, there is a key difference. Namely, as a function of resolution, diffraction from bulk water peaks at around 3.3 Å while diffraction from an all-atom independent motion model (protein or nucleic acid) generally peaks at lower resolution depending on the amplitude of motion of the protein atoms. Thus, each of these components contributes diffracted intensity at different resolutions.

Streaks elongated perpendicular to c^*, surrounding Bragg reflections at high angle in the c^* direction of reciprocal space (red arrows in Figs. 2*a* and 3*a*), were calculated using the convolution method [equation (1)]. The best fit to the observed shapes was achieved using equation (2) with correlation distances of 30, 30 and 130 (10) Å for γ_x, γ_y and γ_z, respectively. The component of this displacement is directed along c^*, *i.e.* the direction of δ for this component is (0,0,1), giving intensity in appropriate regions of reciprocal space. Because the acceptor stems are 60 Å in length and the correlation distance, γ_z, is 130 Å, this suggests that two adjacent tRNA molecules move as a unit along the *c* axis. Correlation along the other two axes is much less coupled (30 Å). Anticodon arms in adjacent unit cells contact each other resulting in the 113 Å unit-cell length along the *a* and *b* axes. This distance is considerably larger than the observed correlation distance of 30 Å. Standard crystallographic analysis shows the terminal half of the anticodon loop region to be highly disordered, thereby suggesting a mechanism for the limited correlation seen in this direction.

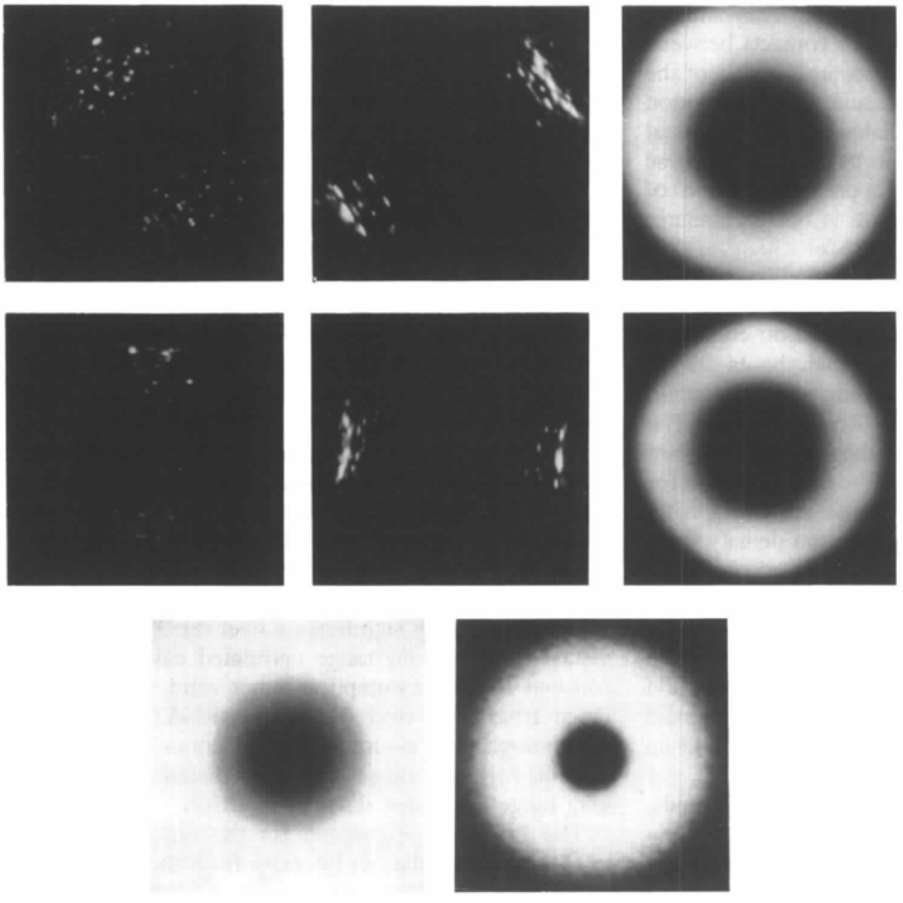

Fig. 4. Diffuse scattering components used in each of the calculations, Figs. 2(*b*) (row 1) and 3(*b*) (row2). Rows 1 and 2: (from left to right) long-range lattice-coupled motion perpendicular to the *c* axis, long-range lattice-coupled motion along the c axis, and short-range motion local to the anticodon arm. Row 3: calculated scattering from bulk water (left) and independent atom motion scattering (right).

In addition to the streaks oriented perpendicular to the c^* axis, there are also halos around Bragg reflections in the $hk0$ plane in the 3-3.5 Å resolution range. Thus, there is also a long-range correlated component due to disorder in the *ab* plane of the unit cell. When viewed down the *c* axis, the projection of the tRNA molecules exhibits hexagonal packing. Two-dimensional colloidal crystals with a similar hexagonal packing have particle displacements that can be factored into three components, each strongly correlated along a principal hexagonal axis, yet weakly correlated in the perpendicular direction (Clarage, 1992). Each tRNA pseudo-helix (lying along the *c* axis) has contacts with neighboring pseudo-helices along three directions. These contacts would allow motion to be transmitted from one pseudo-helix to an adjacent pseudo-helix along one of these three hexagonal lattice directions. By analogy to the colloidal crystal analysis, we factored the tRNA *ab* plane disorder into three components each with component displacement, δ_i, along the principal hexagonal directions and with a corresponding anisotropic correlation function. The refined value of γ_z = 110 (10) Å shows that the correlation along the lattice directions is large; this distance is comparable to the 113 Å separation between pseudo-helices that contact each other. The correlation along directions orthogonal to the axes of contact was determined to be $\gamma_x = \gamma_y$ = 55 (10) Å. This smaller value probably arises from the lack of contacts between adjacent pseudo-helices in these directions and is of the same order as the width of the molecule. The convolution of the three components gives halos at the reciprocal locations mentioned above. While calculation of these halos produces intensity in the appropriate region of reciprocal space, this diffuse feature is not particularly well accounted for by the current model.

In a first attempt to account for the very diffuse clouds of scattering (white arrows in Figs. 2*a* and 3*a*), the multi-cell method was used. One calculation contained the diffraction from a model in which bases 22-46 of the anticodon arm region move as a rigid domain independently from the rest of the tRNA molecule. The amplitude of motion was taken as the root-mean-square (r.m.s.) displacement derived from the mean *B* value for the anticodon loop region. The diffuse scattering from two hundred unit cells containing electron density from the rigidly perturbed unit was calculated according to (4). The results did not correspond well with the actual data, showing more spatial modulation in the intensity than was observed. A second model was tried in which only the three bases, 34-36, at the tip of the anticodon loop moved as a rigid unit. The calculated scattering did show less modulation, but the intensity did not build up in appropriate regions of reciprocal space.

In another attempt to calculate the very diffuse clouds, we used the convolution method in (1) and (2) with an isotropic correlation distance of γ = 6 Å. This model has been used successfully for calculating the very diffuse scattering from both insulin and lysozyme crystals (Caspar, Clarage, Salunke & Clarage, 1988; Clarage, Clarage, Phillips, Sweet & Caspar, 1992). Since this method has worked for two separate protein crystals, we were curious as to whether the 6 Å coupling distance would also apply to tRNA crystals. The calculation proved to be inappropriate for tRNA crystals showing too much spatial modulation in the diffuse intensity and a failure to localize features as observed in reciprocal space.

To localize the calculated diffuse scattering properly, the convolution method was extended to include only portions of the molecule. Ideal structure factors, F_o, were calculated from two portions of the anticodon arm, specifically, bases 22 through 46 as well as bases 8 through 48. These two helical segments were chosen because they exhibit the greatest degree of disorder based on the crystallographic *B* values and because their helical transforms would be prominent in the same positions of reciprocal space as the diffuse clouds. Using a correlation distance of γ = 6 Å diffuse scattering calculations showed that the 8 through 48 base region (see Fig. 1) showed better correspondence with the observed data than the 22 through 46 region. The best agreement with the observed data, however, was achieved by reducing the correlation distance to 3 (1) Å. This distance compares favorably with the base-pair stacking distance of approximately 2.7-3.0 Å in A-form double-helical ribonucleic acid polymers (Saenger, 1984). Thus locally coupled motions of adjacent bases in the 8 through 48 base region of the tRNA molecule would explain the very diffuse features (see Fig. 6).

One important difference between the very diffuse and long-range correlated calculations is the meaning of the ideal structure factor, F_o, used in subsequent convolutions with the halo function. For the short-range calculations, use of the standard F_o produced acceptable results as in previous studies. For the long-range correlations, however, calculations using F_o's without *B* values did not resemble the data at close inspection. Rather, structure factors generated using individual atomic *B* values were used to calculate the diffuse streak intensity. The convolution method generally assumes that *B* values over the entire molecule are all the same. However, in this case, because the moving unit is the entire molecule, F_o must reflect the varying contribution of the atoms according to their individual *B* values. Whereas *B* values do not vary significantly over the 3 Å correlation distance, in the long-range correlated calculations this constant *B* value assumption is not valid. The *B* values range from 2 to over 100 Å^2 in tRNA. As a result, the homogeneous assumption in the convolution method is valid for short-range correlated disorder but not for long-range correlated disorder in tRNA.

The first-order expansion for the diffuse scattering in (1) represents the net intensity from the independent

components of the disorder as a linear combination of the diffuse scattering from these individual components. Thus, because of the $(2\pi\mathbf{R}\cdot\delta_i)^2$ dependence in each scattering component, the relative scale factors used in summing those diffuse scattering contributions (the lattice-coupled and the local anticodon disorder) calculated using the convolution method equal the relative contributions to the total atomic mean-square displacement from these respective components. In our calculations, the δ_i were all treated as unit vectors; in this way the relative magnitudes of the component mean-square displacements, δ_i^2, could be inferred from the ratios between the scale factors. From our fits to the X-ray data, the 3 Å intramolecular liquid-like motion in the anticodon stem has a 17-fold greater mean-square atomic displacement than the two lattice-coupled components. This order of magnitude dominance of short-range over long-range atomic displacements is consistent with X-ray diffuse scattering measurements on insulin, lysozyme and tropomyosin crystals, as well as with time-resolved inelastic scattering measurements on myoglobin crystals. The diffuse streak intensity due to long-range coupled displacements dominates the diffraction pattern only because it is concentrated in a smaller volume of reciprocal space than the intensity due to intramolecular displacements. Of course, as in the case of displacement magnitudes derived from crystallographic B values, the displacements encompassed in X-ray diffuse scattering studies do not include modes longer than the reciprocal of the Bragg spot dimension (typically 5–10 lattice constants).

To obtain absolute magnitudes for the atomic displacements, we fit our calculated anticodon scattering ring to the observed radial distribution of the ring by adjusting the total mean-square displacement from all components, $\Sigma_i\delta_i^2$, in the global Debye–Waller factor $\exp[-\Sigma_i(2\pi\mathbf{R}\cdot\delta_i)^2]$ in (1). The best fit was obtained by using a value of 0.5 Å for $\Sigma_i\delta_i^2$. This value corresponds to a B value of approximately 20 Å^2 which is smaller than the mean B value for tRNA but is consistent with that from typical macromolecules in solvated crystals. Studies indicate that when B values get very large, the atomic distribution is no longer harmonic but is composed of multi-modal substates (Clarage & Phillips, 1994; Kuriyan, Petsko, Levy & Karplus, 1986). Each local well has harmonic movement with $B \simeq 20$ Å^2. Perhaps the diffuse scattering reflects the magnitude of motion within these local wells.

Flexibility appears to be an important component in the design of tRNA and its function. Rould *et al* have shown by X-ray crystallography that the anticodon region of $tRNA^{Gln}$ in *E. coli* changes conformation when bound to its aminoacyl-tRNA synthetase (Rould, Perona, Söll & Steitz, 1989; Rould, Perona & Steitz, 1991). Flexibility of the anticodon region, thus, seems to be important in making contacts with the synthetase in the process of recognition. Conformational changes in tRNA molecules have also been implicated in various processes during protein synthesis. Specifically, changes in the angle between the acceptor and anticodon arms of tRNA

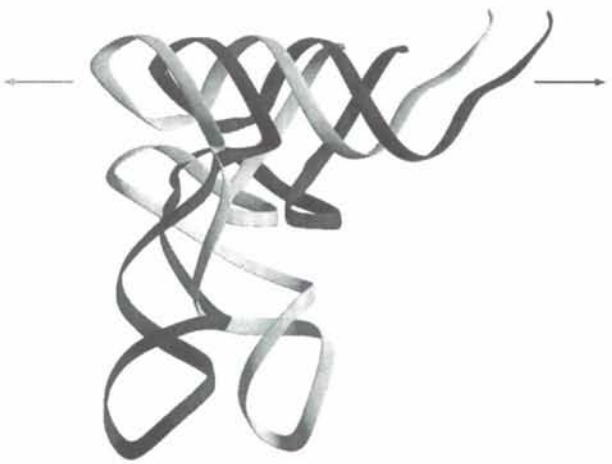

Fig. 5. Ribbon drawing of two tRNA molecules illustrating the possible flexing behavior of tRNA derived from analysis of the Bragg-associated diffuse scattering. Specifically, motion strongly coupled along the pseudo-helical axis (marked by arrows), but relatively uncorrelated with the distal half of the anticodon arm, results in the flexion. The motion along the direction of the arrows has been exaggerated to demonstrate the flexing action better.

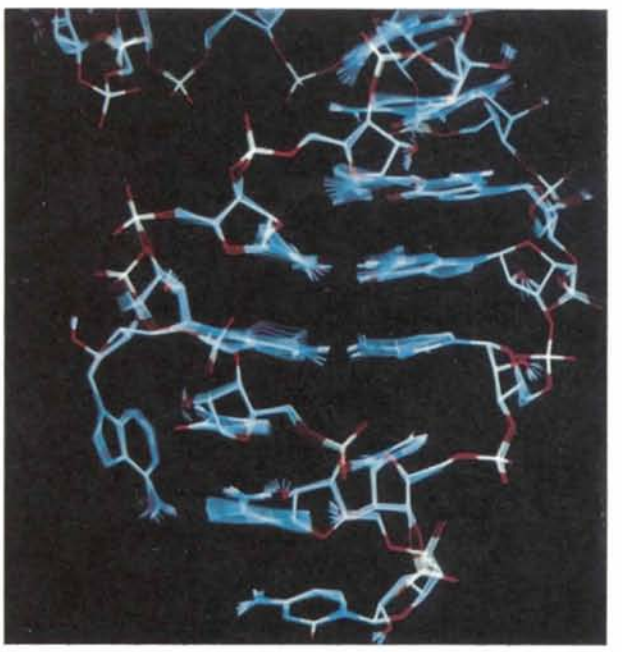

Fig. 6. Schematic stick figure animation illustrating local motion of base pairs in the anticodon loop (separated by approximately 3.0 Å). This picture is based upon information derived from the analysis of the very diffuse clouds in Figs. 2(*a*) and 3(*a*) (white arrows). This representation illustrates the local motion of the nucleic acid bases while still preserving the approximate base-pair separation.

are thought to accompany the transfer of an incoming amino acid to the nascent peptide chain (Spirin, 1987). A similar angular change is implicated in driving mRNA through the ribosome (Nygard & Nilsson, 1990). The anticodon loop has also been shown to change conformation during codon binding. Furthermore, this change appears to influence the conformation in the hinge region connecting the acceptor and anticodon arms (Rigler & Wintermeyer, 1983).

Diffuse scattering analysis can provide information about the types of motion mentioned in the previous paragraph. The diffuse streaks, due to lattice-coupled atomic displacements, were calculated using the convolution method with anisotropic correlation lengths of 130 Å along the pseudo-helix axis and 30 Å perpendicular to this axis. Physically, this corresponds to acceptor arms moving quite rigidly along their helical axes but in a manner relatively uncorrelated with the distal half of their anticodon arms. This disorder implies a flexing motion between the acceptor and anticodon arms (see Fig. 5). Using the same convolution method for only the atoms in the anticodon arms, the diffuse clouds were calculated using an isotropic correlation length of 3 Å. Thus the short-range intramolecular disorder is coupled over a distance which is the order of the base-pair separation within the distal half of the anticodon arm. This coupling can be visualized as concerted motion between neighboring nucleic acid bases within the anticodon arms and signals significant local plasticity in this portion of the nucleic acid (see Fig. 6). Thus, the types of motions postulated to occur during tRNA action do occur in the crystal environment. Moreover, this information could not be obtained by standard crystallographic analysis.

The average structure provided by analysis of Bragg data is a very useful but static model. Analysis of the diffuse scattering, on the other hand, can reveal the dynamic nature of the molecules within the crystal. In yeast initiator tRNA crystals, diffuse scattering analysis reveals both long-range correlated motions of whole molecules and short-range correlated motions within the anticodon arm. In this case and in general, a model that includes variations from the average structure more accurately depicts the molecular features crucial to understanding function.

We would like to thank Professor P. Sigler and Dr R. Basavappa for the yeast initiator tRNA diffraction data and structural coordinates, and the Rigaku Corporation for instrumentation support. This work was supported by grants Welch C-1142 (GNP), NSF DMB 87-16507 (GNP), NIH Training Grant (ARK), NIH NRSA Postdoctoral Fellowship GM-13945 (JBC), and the W. M. Keck Center for Computational Biology.

References

BASAVAPPA, R. (1991). PhD thesis, Yale Univ., New Haven, USA.
BASAVAPPA, R. & SIGLER, P. (1991). *EMBO J.* **10**, 3105-3111.
BOYLAN, D. & PHILLIPS, G. (1986). *Biophys. J.* **49**, 76-78.
CARSON, M. (1987). *J. Mol. Graphics*, **5**, 103-106.
CASPAR, D., CLARAGE, J., SALUNKE, D. & CLARAGE, M. (1988). *Nature (London)*, **332**, 659-662.
CHACKO, S. & PHILLIPS, G. JR (1992). *Biophys. J.* **61**, 1256-1266.
CLARAGE, J., CLARAGE, M., PHILLIPS, W., SWEET, R. & CASPAR, D. (1992). *Proteins*, **12**, 145-157.
CLARAGE, J. & PHILLIPS, G. JR (1994). *Acta Cryst.* D**50**, 24-36.
CLARAGE, M. (1992). PhD thesis, Brandeis Univ., Waltham, Massachusetts, USA.
DOUCET, J. & BENOIT, J. (1987). *Nature (London)*, **325**, 643-646.
DOUCET, J., BENOIT, J., CRUSE, W., PRANGE, T. & KENNARD, O. (1989). *Nature (London)*, **337**, 190-192.
FORSYTH, J. & WELLS, M. (1959). *Acta Cryst.* **12**, 412-415.
FRAUENFELDER, H., PETSKO, G. & TSERNOGLOU, D. (1979). *Nature (London)*, **280**, 558-563.
GLOVER, I., HARRIS, G., HELLIWELL, J. & MOSS, D. (1991). *Acta Cryst.* B**47**, 960-968.
GROS, P., VAN GUNSTEREN, W. & HOL, W. (1990). *Science*, **249**, 1149-1152.
KOLATKAR, A., CLARAGE, J. & PHILLIPS, G. (1992). *Rigaku J.* **9**, 4-8.
KOLATKAR, A., PHILLIPS, G., BASAVAPPA, R. & SIGLER, P. (1990). *Abstr. Am. Crystallogr. Assoc.* **18**, 94.
KURIYAN, J., OSAPAY, K., BURLEY, S., BRÜNGER, A., HENDRICKSON, W. & KARPLUS, M. (1991). *Proteins*, **10**, 340-358.
KURIYAN, J., PETSKO, G., LEVY, M. & KARPLUS, M. (1986). *J. Mol. Biol.* **190**, 227-254.
MORGAN, J. & WARREN, B. (1938). *J. Chem. Phys.* **6**, 666-673.
NIENHAUS, G., HEINZLAND, J., HUENGES, E. & PARAK, F. (1989). *Nature (London)*, **338**, 665-666.
NYGARD, O. & NILSSON, L. (1990). *Eur. J. Biochem.* **191**, 1-17.
PARAK, F., HARTMANN, H., AUMAN, K., REUSCHER, H., RENNEKAMP, G. & BARTUNIK, H. (1987). *Eur. Biophys. J.* **15**, 237-249.
PETSKO, G. & RINGE, D. (1984). *Annu. Rev. Biophys. Bioeng.* **13**, 331-371.
PHILLIPS, G., FILLERS, J. & COHEN, C. (1980). *Biophys. J.* **10**, 485-502.
RIGLER, R. & WINTERMEYER, W. (1983). *Annu. Rev. Biophys. Bioeng.* **12**, 475-505.
ROULD, M., PERONA, J., SÖLL, D. & STEITZ, T. (1989). *Science*, **246**, 1135-1142.
ROULD, M., PERONA, J. & STEITZ, T. (1991). *Nature (London)*, **352**, 213-218.
SAENGER, W. (1984). *Principles of Nucleic Acid Structure*. New York: Springer-Verlag.
SPIRIN, A. (1987). *Biochimie*, **69**, 949-956.
TEN EYCK, L. (1977). *Acta Cryst.* A**33**, 486-492.